Journal of
Materials Chemistry B

PAPER

View Article Online
View Journal

Cite this: DOI: 10.1039/c6tb00897f

Size-controllable ultrathin carboxylated polypyrrole nanotube transducer for extremely sensitive 17β-estradiol FET-type biosensors†

Wonjoo Na, Jin Wook Park, Ji Hyun An and Jyongsik Jang*

17β-Estradiol is known as a steroid hormone in the human body but it is also known as a disruptor that can cause disequilibrium and dysfunction of the human immune system. Recently, there has been much interest in developing biosensors to detect low concentrations of 17β-estradiol. In this work, size-controllable aptamer conjugated ultrathin carboxylated polypyrrole nanotubes (A-UCPPyNTs) were fabricated as transducers in 17β-estradiol field-effect transistor (FET)-type biosensors. They were manufactured *via* a self-degradation method under several different conditions to control the diameter of the nanotubes. For targeting 17β-estradiol, the binding aptamers were immobilized through covalent bonding on its surface. The resulting A-UCPNT FET-type biosensor demonstrated p-type behavior with outstanding electrical conductivity, and exhibited Ohmic contacts between the samples and electrodes. The smaller diameter (40 nm) of ultrathin carboxylated polypyrrole nanotubes (UCPPyNTs) contributed to the biosensor's enhanced performance by generating a larger surface area, thereby increasing the number of conjugated binding aptamers. In conclusion, the A-UCPPyNT FET-type biosensor showed extremely high sensitivity (~1 fM) toward 17β-estradiol, approximately 10^3 times more sensitive than the results found in other reports. Moreover, the A-UCPPyNT FET-type biosensor showed unique selectivity to the 17β-estradiol molecule, in addition to outstanding reusability and long-term storage stability (4 weeks of duration achieved in this work). These performances concerned with reusability and stability were achieved by the formation of covalent bonding in the anchorage to the substrate electrode. Thus this study can be effectively applied in biological and environmental fields.

Received 11th April 2016,
Accepted 24th June 2016

DOI: 10.1039/c6tb00897f

www.rsc.org/MaterialsB

1. Introduction

17β-Estradiol is a steroid molecule that exists not only in the human body but also in various environmental media.[1–5] Within the human body, 17β-estradiol is the most active female sex hormone produced in the ovaries, which plays a crucial role in the normal menstrual cycle, the formation of secondary sexual characteristics, and bone growth.[6–8] However, 17β-estradiol is also known as a disruptor that can cause disequilibrium in hormone immunity and dysfunction of physiological processes.[9–12] When humans are exposed to 17β-estradiol at even low concentrations that exist in our surroundings through wastewater or sewage, it plays a role in increasing the risk of developing several critical diseases such as breast, ovarian, and prostate cancer.[13–15] So establishing a highly sensitive 17β-estradiol determination has been an important research goal in recent years. In recent years, considerable research efforts have been focused on constructing many 17β-estradiol sensing methods, including liquid chromatography (LC),[16,17] fluorescence immunoassay,[18,19] gas chromatography-mass spectrometry (GC-MS),[20,21] electrochemical immunoassay,[22–26] and so on. Although these analysis methods have been useful, it is necessary to simplify the implementation of 17β-estradiol detecting sensors due to their multiple steps of preparation for measurement. Furthermore, higher sensitivity and selectivity for 17β-estradiol are demanded in sensor devices for use in realistic applications.

Aptamers are synthetic single-stranded DNA or RNA sequences randomly selected from the nucleic acid libraries. They present unique characteristics of stability and specificity, easy chemical synthesis, and affinity, and versatility regarding target molecules. These features make aptamers an alternative to antibodies or enzymes. Furthermore, aptamers can be modified with several functional groups, which are capable of being attached on the surfaces of materials both directly and indirectly.[27]

A field-effect transistor (FET) is a transistor that uses an electric field to control the electrical conductivity of one type of charge carrier in a semi-conductor material. This type of transistor

School of Chemical and Biological Engineering, Seoul National University, 1 Gwanak-ro, Gwanak-gu, Seoul 151-742, Korea. E-mail: jsjang@plaza.snu.ac.kr; Fax: +82-2-888-1604; Tel: +82-2-880-7069

† Electronic supplementary information (ESI) available. See DOI: 10.1039/c6tb00897f

has high input impedance that attracts or repels charge carriers to or from the terminals. The current amplification properties achieved in FET-type biosensor devices improve their measuring accuracy, thus increasing the advantages in detecting low concentrations of analytes.[28–32] In some recent research, one-dimensional (1D) nanomaterials that have superb charge carrying mobility along the long-axis are used in various sensor systems to increase the density of charge carriers and enhance the conductivity between the source and drain electrodes.[33–38] Nowadays, conducting polymers (CPs) are actively studied in order to produce nanomaterials due to their distinctive optical, electrical, and mechanical properties.[39–45] Particularly, 1D CP nanostructures – such as nanowires, nanofibers, nanobelts, and nanotubes – are widely synthesized using several polymerization methods.[46–48] These nanostructures are normally used in biosensors due to their biocompatibility and nontoxic properties. However, those numerous fabricating methods have multiple steps, complicated processes, and are difficult to produce on a large scale. Among the various methods used to produce 1D CP nanostructures, the self-degradation method is the most facile method for synthesizing nanotubes (NTs), which does not require additional steps for removing templates.[49] This method also allows large-scale production because it is solvent-based synthesis and it also has simple steps. In FET-type biosensors, CP NTs are used as transducers that convert electrical energy into signal, which plays a key role in the sensing performance of the device. The sensitivity of the FET-type biosensor depends on the surface area and the unit size of the transducer, which requires a thinner and more uniform size of CP NTs. Therefore, controlling the diameter of CP NTs is required during fabrication *via* the self-degradation method to improve the strength and make up for the weakness.

Herein, we describe the fabrication of a 17β-estradiol FET-type biosensor based on size-controllable ultrathin carboxylated polypyrrole nanotubes (UCPPyNTs) conjugated with 17β-estradiol binding aptamers. UCPPyNTs were successfully fabricated *via* a self-degradation method, while the temperature and molar ratio of reactants were under control. The diameters of UCPPyNTs were 40, 70, and 120 nm. They were immobilized on the electrode surface as transducers and conjugated 17β-estradiol aptamers were attached on the surface of UCPPyNTs by covalent bonding. The real-time response of the liquid-ion-gated 17β-estradiol FET-type biosensor was less than 1 s. The limit of detection of this biosensor was 1 fM, which was almost 10^3 times more sensitive than the results in other previous reports. It also showed impressive selectivity towards 17β-estradiol as well as outstanding reusability and storage stability.

2. Experimental section

2.1 Materials

Pyrrole (98%), pyrrole-3-carboxylic acid (P3CA), methyl orange, iron chloride ($FeCl_3$, 97%), (3-aminopropyl)triethoxysilane (APTES), 4-(4,6-dimethoxy-1,3,5-triazin-2-yl)-4-methylmorpholinium chloride (DMT-MM), 17β-estradiol (≥98%), bisphenol A (≥99%), progesterone (≥99%), estriol (≥97%), and cholesterol (Sigma Grade, ≥99%) were purchased from Sigma-Aldrich Co. and used without further purification. The 17β-estradiol binding aptamer was from Bioneer Co. (Dajeon, Korea). The 17β-estradiol binding aptamer was modified at the 5′ terminus with an amine group, and its sequence was as follows: 5′-NH_2-$(CH_2)_6$-GCT TCC AGC TTA TTG AAT TAC ACG CAG AGG GTA GCG GCT CTG CGC ATT CAA TTG CTG CGC GCT GAA GCG CGG AAG C-3′.[50]

2.2 Fabrication of UCPPyNTs

The UCPPyNTs were prepared by the self-degradation method.[46] In the fabrication of 40 nm UCPPyNTs, 1.5 mmol $FeCl_3$ solution was added into 30 mL of 5 mM solution of sodium 4-[4′-(dimethylamino)phenyldiazo]phenylsulfonate, methyl orange (MO), in deionized water. Then, 0.05 mM P3CA and 1.5 mM pyrrole monomer solutions were added and the mixture was stirred at 10 °C for 12 h. The resulting black precipitate was purified by washing with deionized water several times until the filtrate became transparent. The powdered UCPPyNTs thus obtained (0.8 g) were then dried under vacuum at 40 °C for 12 hours. The yield of UCPPyNTs was 79%.

2.3 Fabrication of the A-UCPPyNT FET-type biosensor

The IDA substrate was patterned by using a photolithographic process. A micro-array of 80 pairs of Au interdigitated microelectrodes on a glass substrate using a 50 nm-thick Cr adhesion layer was patterned. The resulting electrodes were formed on a 50 nm-thick, 10 μm-wide, and 4 mm-long Au–Cr layer with 10 μm inter-electrode spacing. To construct the A-UCPPyNT FET-type biosensor platform, the IDA electrode was treated with 5 wt% aqueous APTES for 6 h to introduce amino groups onto the surface of the glass substrate. Then, a mixture of 1 wt% UCPPyNTs (5 μL) in water and 1 wt% aqueous DMT-MM (5 μL) was dropped onto the electrodes. After the electrodes were completely dried, the coupling reaction to attach the 17β-estradiol binding aptamer onto the UCPPyNT surface was carried out using a mixture of 1 μM 17β-estradiol binding aptamer and 1 wt% aqueous DMT-MM (5 μL) for 12 h. The resulting FET-type biosensor substrate based on a liquid-ion gate was fabricated with PBS, with a pH of 7.5. The current was monitored using a source meter device at room temperature.

2.4 Instrumentation

Transmission electron microscope (TEM) images and X-ray photoelectron spectroscopy (XPS) spectra were obtained using a JEM-2100 (JEOL) and a Sigma probe respectively at the National Center for Inter-University Research Facilities (NCIRF) at Seoul National University. Field emission scanning electron microscope (FE-SEM) images were obtained using a JSM-6701F (JEOL). Raman spectra were taken using a T64000 (Horiba Jobin Yvon). Fourier-transform infrared (FT-IR) spectra were collected using a Thermo Scientific Nicolet 6700 FT-IR spectrophotometer. X-ray diffraction (XRD) patterns were collected using a New D8 Advance (Bruker). Brunauer–Emmett–Teller (BET) surface areas were measured using an ASAP 2010 analyzer (Micrometrics). All electrical measurements were carried out using a Keithley 2612A

source meter, a probe station (MS TECH, model 4000) and a WBCS 3000 potentiostat (Wonatech).

3. Result and discussion

3.1 Mechanism of UCPPyNT formation

Fig. 1a shows the overall procedure for the fabrication of UCPPyNTs using the self-degradation method. The self-degradation method is a facile synthesis method, which uses self-degraded fibrillar templates composed of methyl orange (MO) and iron chloride ($FeCl_3$). It is known that MO cannot act as a surfactant because it lacks critical micelle concentration (CMC) though it has a planar conformation with both hydrophobic part and hydrophilic sulfite group. In this method, $FeCl_3$ acts as both an oxidant and a cohesive agent that can neutralize the electrostatic repulsive forces between the negatively charged sulfite ion of MO and the Fe^{3+} ion in the solution. This phenomenon leads to the formation of MO–$FeCl_3$ fibrillar templates (Fig. S1, ESI†).

Polymerization of pyrrole/pyrrole-3-carboxylic acid monomers (carboxylated pyrrole monomers, CPys) onto the MO–$FeCl_3$ template occurs through two different routes. In the first route, CPys interact with the fibrillar template due to the electrostatic interaction between the pyrrole monomer and the sulfite group of MO. At the same time, the reaction between CPys and Fe^{3+} cations begins on the surface of the fibrillar template. The polymerization reaction mechanism is as follows:

$$CPy + Fe^{3+} \rightarrow CPy^{+} + Fe^{2+}$$

$$2CPy^{+} \rightarrow CPy\text{–}CPy + 2H^{+}$$

$$CPy\text{–}CPy + Fe^{3+} \rightarrow CPy\text{–}CPy^{+} + Fe^{2+}$$

$$CPy\text{–}CPy^{+} + CPy^{+} \rightarrow CPy\text{–}CPy\text{–}CPy^{+} + H^{+}$$

where CPy^{+} is the carboxylated pyrrole radical cation that can dimerize with the release of a proton.[51]

As polymerization continues, Fe^{3+} cations are changed to Fe^{2+}, which leads to degradation of the template. However, this chain growth reaction normally occurs at the outer surface of the template, so CPys generally react with Fe^{3+} cations that exist in the solution not in the template. Therefore, the degradation of the template from UCPPyNTs takes place through another polymerization route.[52]

The second route of polymerization of CPys takes place inside the template as some CPys can interact with the azo group of MO through hydrogen bonding. In this mechanism, CPys can begin polymerization within the template by reacting with Fe^{3+} cations connected to the MO molecules. This polymerization reaction route breaks down the MO–$FeCl_3$ template due to the decrease of Fe^{3+} concentration. After all these reactions have occurred, UCPPyNTs are finally synthesized.

3.2 Fabrication of UCPPyNTs

To produce UCPPyNTs of various diameters, we varied the molar ratio of monomer/MO/$FeCl_3$ as well as the temperature condition as listed in Table 1. MO–$FeCl_3$ templates were synthesized by mixing MO and $FeCl_3$ in distilled water at 10 °C. Then, CPy monomers (in a 10 : 1 molar ratio of pyrrole : pyrrole-3-carboxylic acid) were added into the template solution and mixed for 12 h. The functional groups of pyrrole-3-carboxylic acid were united

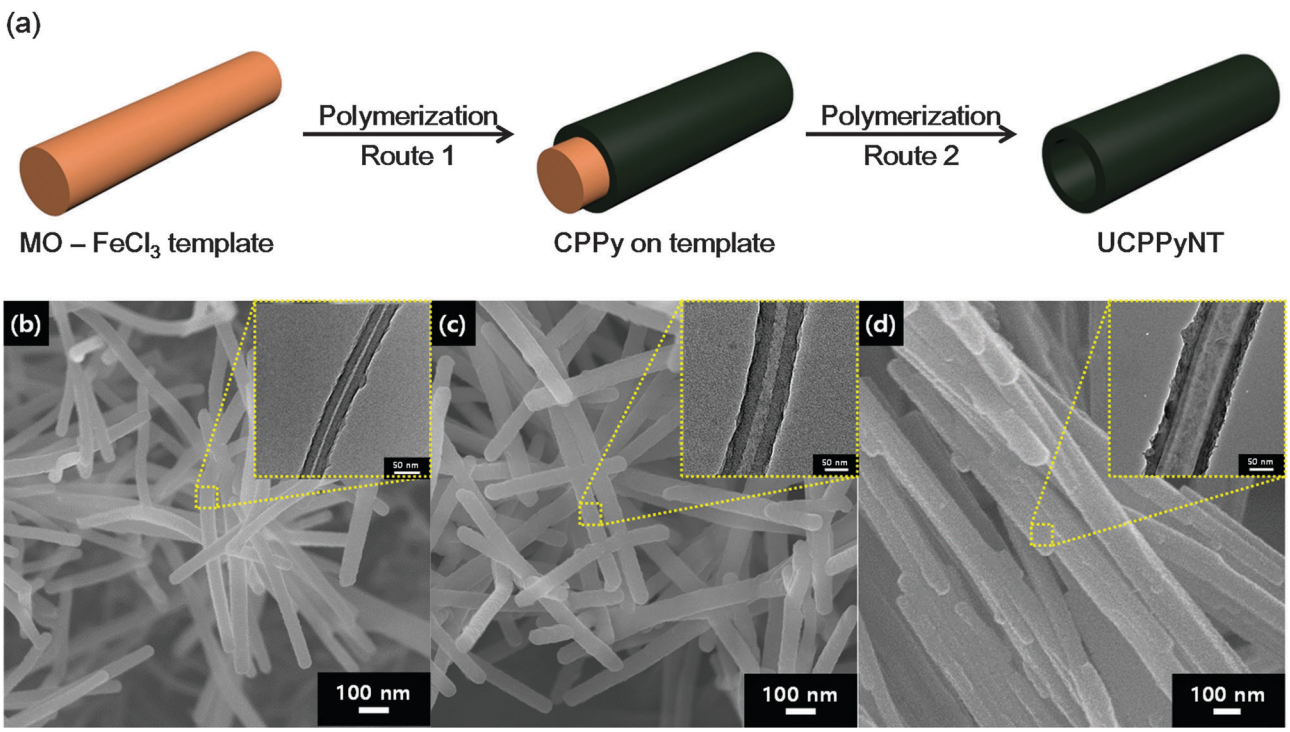

Fig. 1 (a) Illustrative diagram of the sequential fabrication steps for UCPPyNTs. SEM and TEM (inset) images of (b) 40 nm, (c) 70 nm, and (d) 120 nm UCPPyNTs.

Table 1 The molar ratio of reactants and reaction temperature conditions used during the preparation of UCPPyNTs of different diameters

Diameter (nm)	Molar ratio of monomer/MO/$FeCl_3$	Temperature (°C)
40	5 : 1 : 10	10
70	10 : 1 : 10	20
120	20 : 1 : 10	30

with the pyrrole repeating units through α–α′ covalent bonding without any deterioration of their properties. As a result, 40 nm UCPPyNTs were formed, as confirmed by scanning electron microscopy (SEM) and transmission electron microscopy (TEM) images displayed in Fig. 1b. In the same manner, but by varying the temperature and molar ratios of monomer/MO/$FeCl_3$, UCPPyNTs of 70 and 120 nm in diameter were also manufactured as shown in Fig. 1c and d. The wall thicknesses of these UCPPyNTs were about 20–25 nm. When the temperature was not controlled during the fabrication process, the diameters of UCPPyNTs were changed to some degree from 50 to 120 nm. However, the wall thicknesses were simultaneously changed variously from 20 to 40 nm (Fig. S2, ESI†). The lower reaction temperature caused a reduction in the micelle volume due to deactivation of the chain mobility of MO, which reduced the micelle volume and made the diameter of MO–$FeCl_3$ templates smaller. Moreover, the curtailed monomer ratio kept the wall thickness of UCPPyNTs constant. Through regulation of the molar ratio of monomer/MO/$FeCl_3$ as well as the temperature condition, the diameter of UCPPyNTs can be controlled easily with a constant wall thickness.

3.3 Characterization of UCPPyNTs

To provide further insight into the structure of each sample, Fourier-transform infrared (FT-IR) spectroscopy was carried out, as displayed in Fig. 2. Both UCPPyNTs and polypyrrole nanotubes (PPyNTs) had peaks at 1554 cm^{-1} and 1457 cm^{-1}, which indicates the C–C and C–N stretching vibrations in the pyrrole ring, respectively. The peaks at 1294 cm^{-1} and 1031 cm^{-1} were related to the in-plane C–H vibrations. Unlike PPyNTs, a peak at 1733 cm^{-1} was observed in the UCPPyNTs, due to the C═O stretching vibration of the carboxyl groups.[48,49]

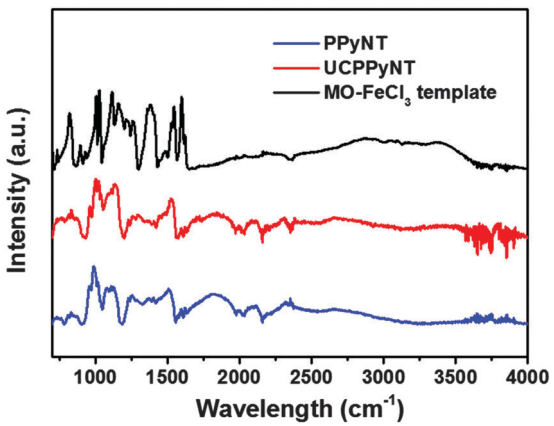

Fig. 2 FT-IR spectra of PPyNTs, UCPPyNTs, and MO–$FeCl_3$ templates.

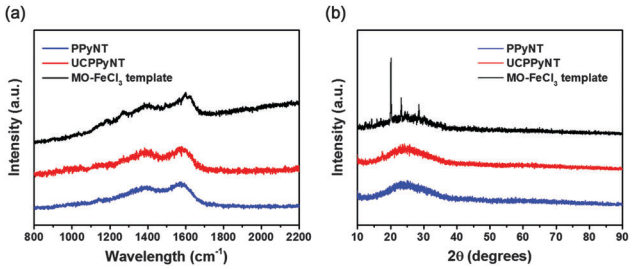

Fig. 3 (a) Raman spectra and (b) X-ray diffraction patterns of PPyNTs, UCPPyNTs, and MO–$FeCl_3$ templates.

Furthermore, the MO–$FeCl_3$ template exhibited several identifiable peaks. The sharp peak observed at 1602 cm^{-1} was associated with the N═N stretching vibration of the azo dye, and the peak observed at 1158–1165 cm^{-1} and the strong peaks at 898 cm^{-1} were associated with the S═O stretching vibration of SO_3^- groups of MO.[52] Furthermore, a broad peak at 3200–3500 cm^{-1} was also observed in the UCPPyNTs, due to the –OH stretching vibration of the carboxyl groups.

Raman spectroscopy was also used to analyse the structural vibration within the bonds in each component, as shown in Fig. 3a. The characteristic peak at 1590 cm^{-1} represents the backbone stretching of C═C bonds in the pyrrole ring, while another strong peak at 1386 cm^{-1} can be ascribed to the C–N stretching of the oxidized polypyrrole.[53]

To examine the crystallinity and the chain packing of the polymer, X-ray diffraction (XRD) analysis was carried out, as indicated in Fig. 3b. The broad peak in the region $20^\circ < 2\theta < 30^\circ$ is the typical peak of amorphous polypyrrole, which can likely be attributed to the π–π interaction of the polypyrrole chain. The intense peak observed at 19.5° reveals the regular array that produces low crystallinity in the structure.[54]

The cyclic voltammetry (CV) test with UCPPyNTs which had different ratios of pyrrole (Py) and pyrrole-3-carboxylic acid (P3CA) from 10 : 1 to 50 : 1 and PPyNTs was carried out (Fig. S3a, ESI†). The CV curves were acquired from −0.4 V to 0.6 V at a scan rate of 5 mV s^{-1} in a 0.1 M PBS electrolyte. As the P3CA content increased, the capacitance increased due to the surface oxygen-containing functional groups (240 mF g^{-1}), the carboxyl group in this case, which led to large pseudocapacitance, less aggregation, and good contact with aqueous solution properties.[55,56] Moreover, the electrochemical impedance spectroscopy (EIS) test was also carried out. As demonstrated in Fig. S3b (ESI†), the diameter of the semi-circle decreased when the ratio of P3CA increased. This result means that the contact resistance with the electrolyte decreased when more carboxyl groups were introduced on the surface of UCPPyNTs. On the other hand, the internal resistance itself increased when the carboxylic acid groups increased on the surface compared with the starting points of the semi-circle during the EIS measurement. The functional groups break the conjugated structure and localize π-electrons, which results in a decrease of both carrier mobility and carrier concentration.[57–60]

Fig. 4 presents the N_2 adsorption/desorption isotherms measured using the Brunauer–Emmett–Teller (BET) method

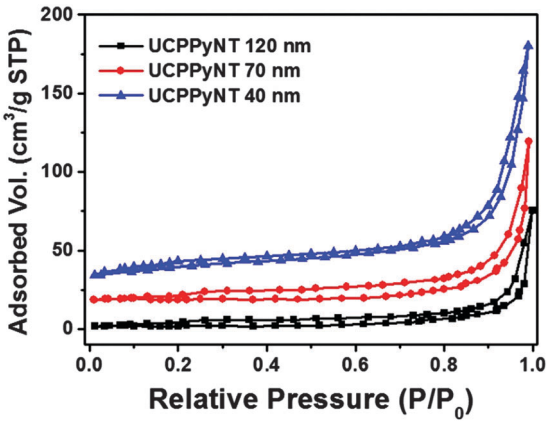

Fig. 4 Nitrogen adsorption–desorption curves for 40, 70, and 120 nm UCPPyNTs. STP represents standard temperature and pressure.

for UCPPyNTs with diameters of 40, 70, and 120 nm, to confirm their specific surface areas. Among the samples, UCPPyNTs with 40 nm diameter had the largest surface area of 81.86 $m^2 g^{-1}$, which was 1.7 and 2.4 times greater than that of UCPPyNTs with 70 nm diameter (57.04 $m^2 g^{-1}$) and 120 nm diameter (39.67 $m^2 g^{-1}$), respectively.

3.4 Fabrication of the A-UCPPyNT FET-type biosensor

The procedure for the attachment of the UCPPyNTs conjugated with the 17β-estradiol binding aptamer on the electrode substrate is described in Fig. 5. An interdigitated microelectrode array (IDA) was patterned on a glass substrate by a lithographic process, composed of 25 pairs of gold finger bands on the glass plate. To functionalize amine groups ($-NH_2$) on the surface of the IDA glass substrate, it was treated with APTES. Subsequently, UCPPyNTs were fastened to the substrate through a condensation reaction between the carboxyl groups (–COOH) of the UCPPyNTs and the amine groups ($-NH_2$) of the APTES-treated IDA glass substrate involving the condensing agent 4-(4,6-dimethoxy-1,3,5-triazin-2-yl)-4-methylmorpholinium chloride (DMT-MM). Thus, the UCPPyNTs were covalently attached on the IDA electrode substrate through a simple chemical reaction. This condensation reaction also enabled the immobilization of the 17β-estradiol binding aptamer to the UCPPyNTs. The carboxyl groups (–COOH) of UCPPyNTs and the amine groups ($-NH_2$) of the aptamer allowed another condensation reaction. The sequence of the 17β-estradiol binding aptamer used was as follows: 5′-NH_2-$(CH_2)_6$-GCT TCC AGC TTA TTG AAT TAC ACG CAG AGG GTA GCG GCT CTG CGC ATT CAA TTG CTG CGC GCT GAA GCG CGG AAG C-3′.[50] As a result of the above reactions, 17β-estradiol binding aptamer-conjugated UCPPyNTs (A-UCPPyNTs) were fabricated on the IDA glass substrate electrode for application as a transducer in FET biosensors. These biosensors had outstanding storage stability and durability for analyte sensing in the liquid phase.

3.5 Characterization of the A-UCPPyNT FET-type biosensor

To evaluate the electrical contact of A-UCPPyNTs on the IDA substrate electrode in the liquid phase, a current–voltage (I–V) curve was monitored in real time. Fig. 6 shows the I–V characteristics of the 40, 70, and 120 nm UCPPyNTs. Nonlinear modulation in an I–V curve indicates the poor electrical contact,

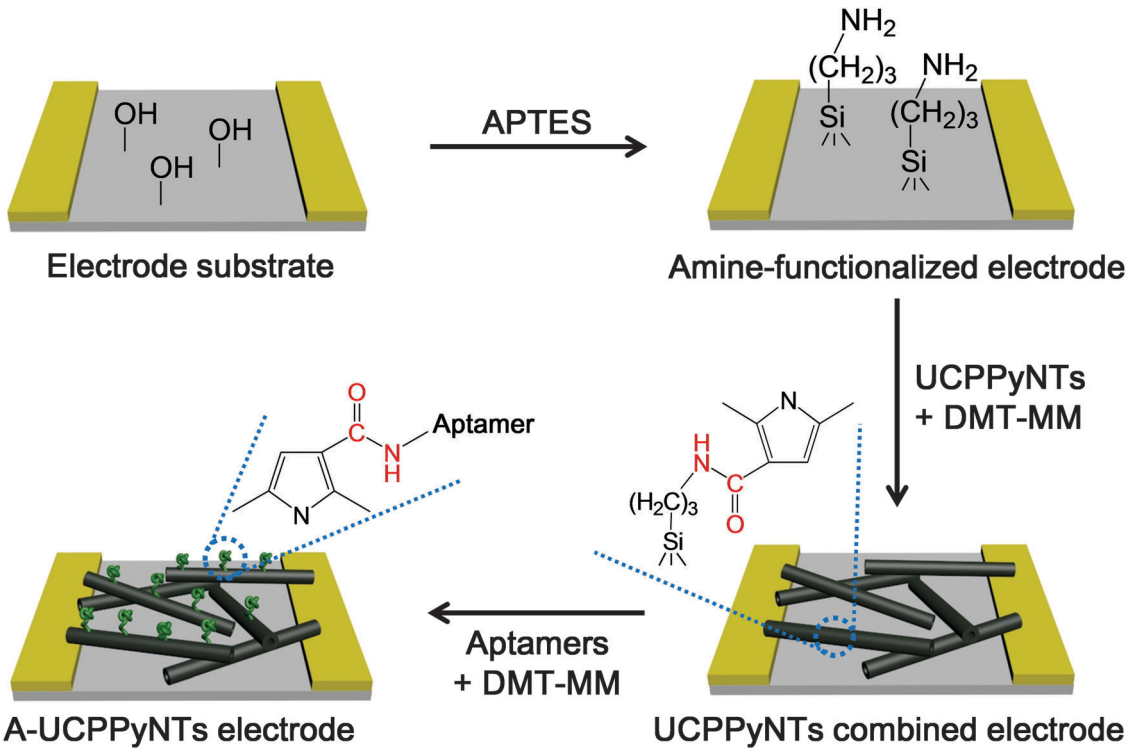

Fig. 5 Schematic diagram of the binding process used to produce the biosensor electrode based on A-UCPPyNTs on the IDA electrode substrate.

likely due to the formation of Schottky barriers at the electrode.[61] However, A-UCPPyNTs exhibited a linear curve, indicating the Ohmic contact of the A-UCPPyNTs covalently bonded on the electrode providing a good electrical contact when the measured voltage ranged from −0.1 to 0.1 V. As the diameter of the UCPPyNTs decreased, the dI/dV values of the electrode slightly increased. In contrast, the dI/dV values decreased when the 17β-estradiol binding aptamer was introduced on the surface of A-UCPPyNTs. This decrease was due to the change in the oxidation level of UCPPyNTs, caused by the separation of elements through condensation reactions. The binding aptamer, which is a nonconductive substance, also played a role in reducing the dI/dV values. Even so, the linearity of the I–V curve was still maintained after introduction of the binding aptamer, which indicates that the 17β-estradiol binding aptamer was effectively conjugated to the UCPPyNTs, with no aggravation of electrical contact and conductivity.

X-ray photoelectron spectroscopy (XPS) analysis was performed to confirm the oxidation level changes due to covalent bonding. As shown in Fig. S4 (ESI†), the deconvolution data of the O 1s peak, the C═O peak at 532.4 eV and the OH^- peak at 534 eV decreased after the immobilization of the 17β-estradiol binding aptamer (the peak at 530.8 eV known as the O^{2-} peak indicated physically absorbed oxygen/carbonates).[62–64] The decrease of C═O and OH^- peaks means that the oxidation level of nanotubes increased and the carboxyl groups were successfully involved in peptide bonding where aptamers were combined on the surface of A-UCPPyNTs.

Fig. 7a provides a schematic diagram of the liquid-ion-gated FET-type biosensor system based on A-UCPPyNTs. This biosensor platform was constructed on the IDA substrate electrode array using A-UCPPyNTs as the conductive channel transducers. The two gold bands were used as the source and drain electrodes. The top gate electrode was submerged in the electrolyte: phosphate-buffered saline (PBS, pH 7.4) solution. To demonstrate the charge transport properties of A-UCPPyNTs in the FET-type biosensor system, the source–drain current (I_{SD}) and voltage (V_{SD}) were monitored while the value of gate voltage (V_G) was varied (Fig. 7b). The I_{SD} value became negative as the V_G value also became more negative. This result is a typical characteristic of hole transporting p-type transistor behavior caused by increasing the oxidation level of the polymer chains.[65] Therefore, the current in this device occurs due to hole transport and changes in the hole carrier density at the surface of A-UCPPyNTs. All these results confirmed that the A-UCPPyNT FET-type biosensor could be effectively used as an electrochemical biosensor for detecting target analytes in a PBS solution.

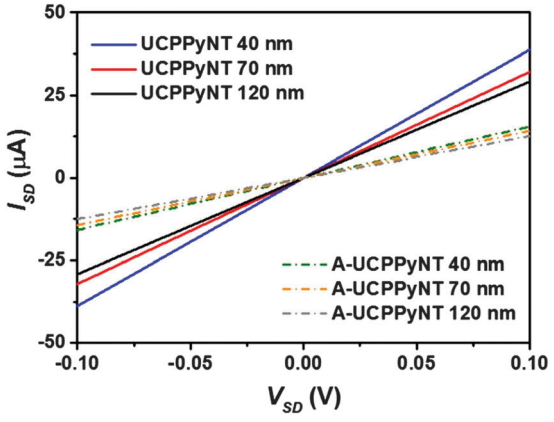

Fig. 6 Source–drain current–voltage (I_{SD}–V_{SD}) curves of the IDA electrode substrates based on 40, 70, and 120 nm UCPPyNTs, compared with before and after the introduction of the 17β-estradiol binding aptamers (V_{SD} scan rate: 0.01 V s^{-1}).

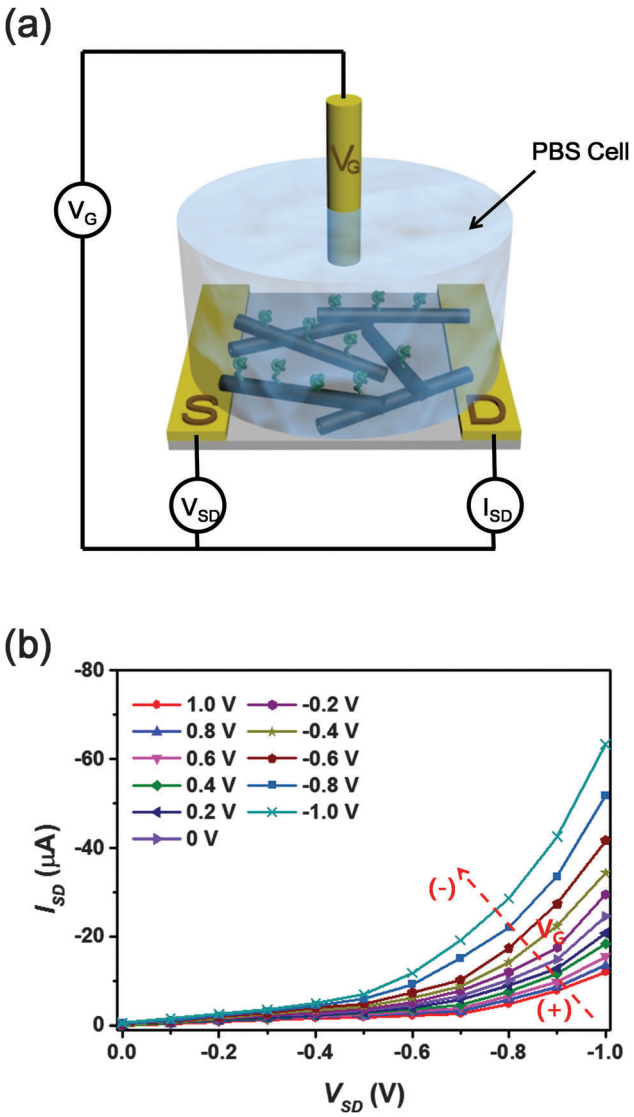

Fig. 7 (a) Schematic diagram of the liquid-ion-gated FET-type biosensor platform with the A-UCPPyNT arrays. (b) Source–drain current *versus* source–drain voltage (I_{SD}–V_{SD}) curves of a 40 nm A-UCPPyNT FET-type biosensor electrode for a varying gate voltage (V_G) ranging from −1.0 to 1.0 V (V_{SD} scan rate: 0.2 V s^{-1}).

3.6 Real-time responses of the A-UCPPyNT FET-type biosensor

The performance of the A-UCPPyNT FET-type biosensor was demonstrated by monitoring the I_{SD} changes that occurred

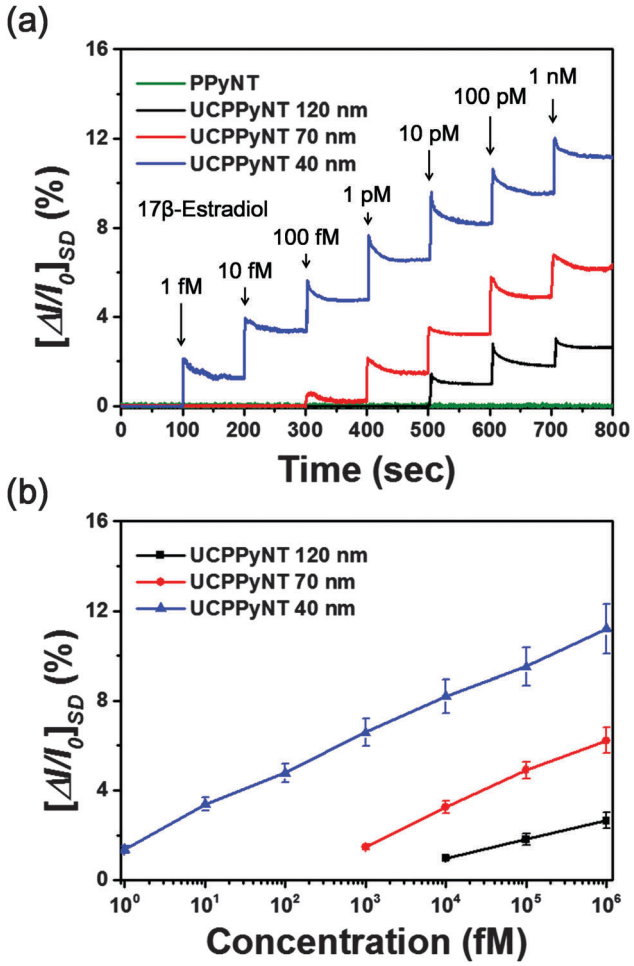

Fig. 8 (a) Real-time responses of the FET-type biosensors of 40, 70, and 120 nm A-UCPPyNTs with normalized current changes. (b) Calibration curves of the real-time response of the FET-type biosensors as a function of 17β-estradiol concentration. The normalized current changes used after 30 s of 17β-estradiol exposure. (V_G: −0.7 V, V_{SD}: 0.01 V).

upon the addition of various concentrations of 17β-estradiol in real time at constant V_{SD} and V_G (−0.8 V). Fig. 8a presents the real-time responses of the A-UCPPyNT FET-type biosensor with different diameters of UCPPyNTs to 17β-estradiol at various concentrations. This biosensor device showed a very fast real-time response, less than 1 s, when adding different concentrations of 17β-estradiol. The conductance dependence on gate voltage enables one to construct an electrical sensing platform based on FET-type biosensors, because an electric field is generated when the charged species bind to the gate dielectric. This electric field generated is similar to applying a gate voltage. Specifically, the binding event between the 17β-estradiol analyte and the aptamer promotes structural rearrangement of the bound aptamer. Thus, it tellingly induces a negatively charged state in the liquid-ion gate dielectric near the A-UCPPyNTs, accumulating positive charge (hole) carriers in the A-UCPPyNT channels. It is similar to the p-type doping effect acting indirectly on the liquid-ion gate dielectric, instead of intimately affecting the semi-conducting layer. Finally, the reinforced negative gate voltage effect from this mechanism caused an increase of I_{SD} for the p-type transducer of UCPPyNTs.[31]

The sensitivity of the A-UCPPyNT FET-type biosensor increased as the NT diameter decreased. That is, the 40 nm A-UCPPyNT was capable of detecting 1 fM 17β-estradiol at room temperature. Distinctively, 70 nm and 120 nm A-UCPPyNTs detected 1 pM and 10 pM 17β-estradiol, respectively. Interestingly, the 70 nm A-UCPPyNT had a peak at 100 fM, but had a signal-to-noise ratio of less than 3 (S/N = 0.95), and there the peak was not considered statistically significant. As a control experiment, identical tests were conducted with the PPyNTs; no obvious current signals were detected. This higher sensitivity performance observed in the smaller-diameter A-UCPPyNTs likely results from the higher proportion of functional covalent bonds between the carboxylic acid group of UCPPyNTs and the amine group of the aptamer, compared with the larger-diameter UCPPyNTs. The results confirm that the 40 nm A-UCPPyNT had a limit of detection (LOD) of 1 fM, indicating that it is almost 10^3 times more sensitive than previously reported optoelectronic and electrochemical 17β-estradiol biosensors, as shown in Table 2.

The calibration curve for the sensitivity of the A-UCPPyNT FET-type biosensor is delineated in Fig. 8b. The sensitivity of the biosensor changes as a function of the diameter of the A-UCPPyNTs with regard to the concentration of 17β-estradiol. The sensitivity was defined by the normalized current change as denoted below:

$$\frac{\Delta I_{SD}}{I_0} = \frac{(I_{SD} - I_0)}{I_0} \quad (1)$$

where I_0 is the initial current value and I_{SD} is the stabilized current value after the addition of different 17β-estradiol concentrations.

The 17β-estradiol biosensor based on 40 nm A-UCPPyNTs had 10^3 times and 10^4 times more sensitivity than that based on 70 nm A-UCPPyNTs and 120 nm A-UCPPyNTs respectively, due to the larger surface area and the increased amount of the active functional group on its surface.

The wide response range of the 17β-estradiol FET-type biosensor was demonstrated until saturated signals appeared (Fig. S5, ESI†). The saturation limit of detection (SLOD) was 10 nM in a real-time response platform.

The selectivity test of the A-UCPPyNT FET-type biosensor towards 17β-estradiol was carried out by real-time monitoring

Table 2 Comparison of the performance of previously reported 17β-estradiol sensors

Sensor type	Limit of detection (pM)	Ref.
Fluorescence immunosensor	220	1
Electrochemical immunosensor	73.4	23
Hydrogel optical waveguide spectroscopy	183.6	66
Colorimetric aptasensor	200	67
Differential pulse voltammetry aptasensor	0.8	50
Surface plasmon resonance spectroscopy	0.25	12
Field-effect transistor-type biosensor	0.001	This work

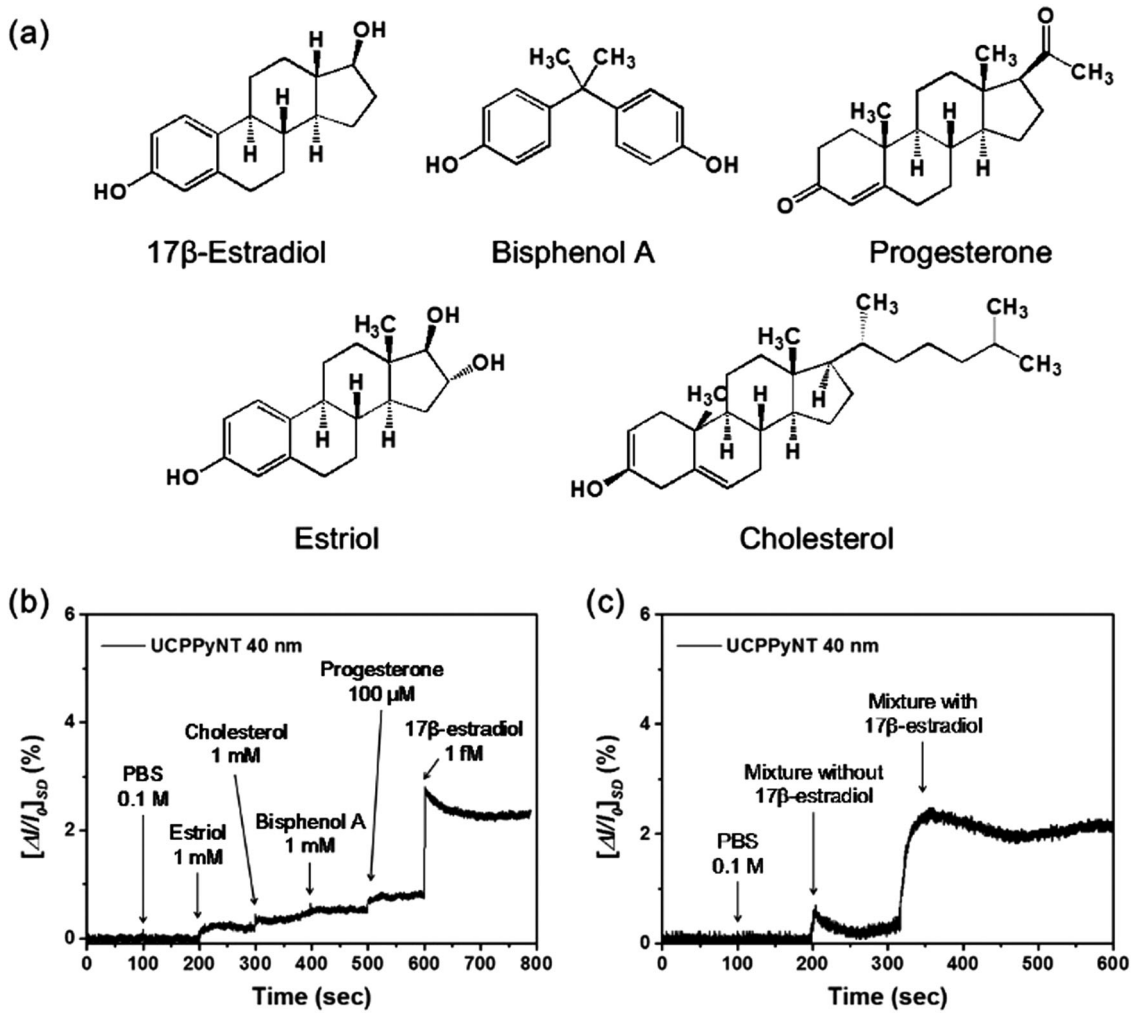

Fig. 9 (a) Molecular diagrams of several structurally similar molecules. (b) Real-time responses for the selectivity test of the 40 nm A-UCPPyNT FET-type biosensor toward non-target (PBS, estriol, cholesterol, bisphenol A, and progesterone) and target (17β-estradiol) analytes. (c) Real-time responses of the 40 nm A-UCPPyNT FET-type biosensor for analytes before and after mixing 17β-estradiol. (V_G: −0.7 V, V_{SD}: 0.01 V).

of I_{SD} changes upon adding several structurally similar molecules: estriol, cholesterol, bisphenol A, and progesterone (Fig. 9a). The A-UCPPyNT FET-type biosensor did not reveal any valid current changes except for 17β-estradiol as presented in Fig. 9b. Several invalid peaks were observed due to the structural similarity of the molecules, which differed in only one group at the end. To further support the selectivity of the A-UCPPyNT FET-type biosensor, a mixture of non-target molecules was added prior to the addition of the non-target/target molecule mixture. Fig. 9c represents the meaningful signal changes after the addition of mixtures containing the target molecule, 17β-estradiol, compared with the result of the addition of mixtures without 17β-estradiol.

One of the major advantages of the covalent-bonding-based FET-type biosensor system is its reusability and storage stability. The evaluation of the reusability of FET-type biosensors based on A-UCPPyNTs of various diameters was carried out with the addition of 1 pM 17β-estradiol over several weeks, as demonstrated in Fig. 10. To prove their reusability, the A-UCPPyNT FET-type biosensors were stored in a sealed petri dish at room temperature

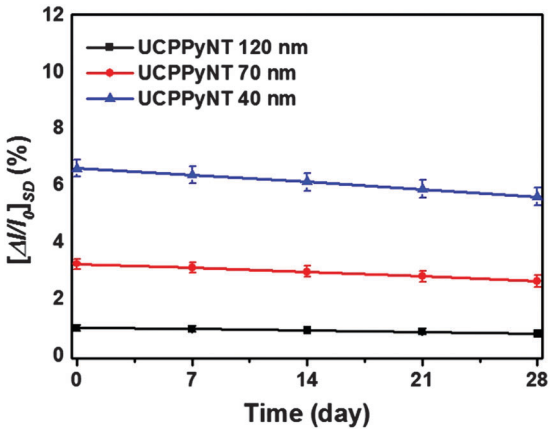

Fig. 10 Storage stability and reusability test comparing 40, 70, and 120 nm A-UCPPyNT FET-type biosensors over 4 weeks. Measurements were taken at 1 week intervals.

under dry conditions for 4 weeks. Under these conditions, the sensitivity decreased to *ca.* 18% after 4 weeks (16%, 19%, and

20% for the 40, 70, and 120 nm A-UCPPyNT FET-type biosensor, respectively). These decreases in sensitivity were due to the inactivation of the binding aptamer or the collapse of the A-UCPPyNT arrays. Nevertheless, the A-UCPPyNT FET-type biosensors maintained their sensing abilities after reuse and storage at room temperature.

4. Conclusion

We demonstrated a highly sensitive and selective A-UCPPyNT FET-type biosensor toward 17β-estradiol. The A-UCPPyNTs were fabricated *via* a self-degradation method under several different conditions to control the diameter of the nanotubes, and subsequently binding aptamers were introduced on their surface through covalent bonding. The resulting A-UCPPyNT FET-type biosensor showed p-type behavior with remarkable electrical conductivity, and formed Ohmic contacts between the samples and electrodes. This is the first demonstration of an aptamer conjugated conducting polymer-based FET-type biosensor specifically targeting 17β-estradiol. The smaller diameter (40 nm) of A-UCPPyNTs contributed to the great performance of the biosensor by generating a larger surface area, thereby increasing the number of conjugated binding aptamers. In consequence, the A-UCPPyNT FET-type biosensor showed extremely high sensitivity ($\sim$1 fM) toward 17β-estradiol, approximately 10^3 times more sensitive than that of other previous reports. Furthermore, the A-UCPPyNT FET-type biosensor exhibited specific selectivity to the 17β-estradiol molecule, as well as excellent reusability and long-term storage stability (4 weeks of duration achieved in this work). These reusability and storage stability properties resulted from the formation of covalent bonding in the fastening to a substrate electrode. Therefore, this study can be effectively applied in biological and environmental fields.

Acknowledgements

This research was supported by the National Research Foundation of Korea (NRF) grant funded by the Korea government (MEST) (Grant No. 2011-0017125).

Notes and references

1 F. Long, H. C. Shi and H. C. Wang, *RSC Adv.*, 2014, **4**, 2935–2941.
2 J. C. Wolf, I. Lutz, W. Kloas, T. A. Springer, L. R. Holden, H. O. Krueger and A. J. Hosmer, *Environ. Toxicol. Chem.*, 2010, **29**, 1091–1105.
3 K. J. Huang, Y. J. Liu, J. Z. Zhang, J. T. Cao and Y. M. Liu, *Biosens. Bioelectron.*, 2015, **67**, 184–191.
4 G. Wang, Y. Wang, L. Chen and J. Choo, *Biosens. Bioelectron.*, 2010, **25**, 1859–1868.
5 K. J. Huang, Y. J. Liu, J. Z. Zhang and Y. M. Liu, *Anal. Methods*, 2014, **6**, 8011–8017.
6 L. Y. Du, W. Ji, Y. F. Zhang, C. Y. Zhang, G. F. Liu and S. H. Wang, *Analyst*, 2015, **140**, 2001–2007.
7 Y. Taes, B. Lapauw, S. Vandewalle, H. Zmierczak, S. Goemaere, D. Vanderschueren, J. M. Kaufman and G. T'Sjoen, *Bone*, 2009, **45**, 392–397.
8 L. Zirilli, V. Rochira, C. Diazzi, G. Caffagni and C. Carani, *J. Steroid Biochem. Mol. Biol.*, 2008, **109**, 212–218.
9 G. Bondar, J. Kuo, N. Hamid and P. Micevych, *J. Neurosci.*, 2009, **29**, 15323–15330.
10 P. X. Huang, V. Chandra and F. Rastinejad, *Annu. Rev. Physiol.*, 2010, **72**, 247–272.
11 N. Sai, Y. T. Wu, Z. Sun, G. W. Huang and Z. X. Gao, *Talanta*, 2015, **144**, 157–162.
12 Y. Tan and T. X. Wei, *Talanta*, 2015, **141**, 279–287.
13 A. H. Eliassen, D. Spiegelman, X. Xu, L. K. Keefer, T. D. Veenstra, R. L. Barbieri, W. C. Willett, S. E. Hankinson and R. G. Ziegler, *Cancer Res.*, 2012, **72**, 696–706.
14 B. Montgomery, P. S. Nelson, R. Vessella, T. Kalhorn, D. Hess and E. Corey, *BMC Cancer*, 2010, **10**, 244.
15 J. Song, A. Fadiel, V. Edusa, Z. Chen, J. So, H. Sakamoto, D. A. Fishman and F. Naftolin, *Cancer Lett.*, 2005, **220**, 57–65.
16 A. Mishra and K. P. Joy, *Gen. Comp. Endocrinol.*, 2006, **145**, 84–91.
17 L. Suna, W. Yong, X. Chu and J.-M. Lin, *J. Chromatogr. A*, 2009, **1216**, 5416–5423.
18 D. Scalas, S. Squadrone, M. Gili, D. Marchis, M. Prearo and M. C. Abete, *J. AOAC Int.*, 2007, **90**, 1427–1431.
19 M. M. Sun, L. Y. Du, S. Q. Gao, Y. H. Bao and S. H. Wang, *Steroids*, 2010, **75**, 400–403.
20 A. K. Tsakalof, D. C. Gkagtzis, G. N. Koukoulis and C. S. Hadjichristodoulou, *Anal. Chim. Acta*, 2012, **709**, 73–80.
21 Y. Zuo, K. Zhang and Y. Lin, *J. Chromatogr. A*, 2007, **1148**, 211–218.
22 K. J. Huang, Y. J. Liu, G. W. Shi, X. R. Yang and Y. M. Liu, *Sens. Actuators, B*, 2014, **201**, 579–585.
23 J. Li, S. Liu, J. H. Yu, W. J. Lian, M. Cui, W. Xu and J. D. Huang, *Sens. Actuators, B*, 2013, **188**, 99–105.
24 Z. Y. Lin, L. F. Chen, G. Y. Zhang, Q. D. Liu, B. Qiu, Z. W. Cai and G. N. Chen, *Analyst*, 2012, **137**, 819–822.
25 M. J. Monorris, F. J. Arevalo, H. Fernandez, M. A. Zon and P. G. Molina, *Sens. Actuators, B*, 2015, **208**, 525–531.
26 L. H. Yuan, J. Zhang, P. Zhou, J. X. Chen, R. Y. Wang, T. T. Wen, Y. Li, X. M. Zhou and H. J. Jiang, *Biosens. Bioelectron.*, 2011, **29**, 29–33.
27 Y. S. Kim, H. S. Jung, T. Matsuura, H. Y. Lee, T. Kawai and M. B. Gu, *Biosens. Bioelectron.*, 2007, **22**, 2525–2531.
28 B. Cai, S. Wang, L. Huang, Y. Ning, Z. Zhang and G. J. Zhang, *ACS Nano*, 2014, **8**, 2632–2638.
29 V. Q. Dang, D. I. Kim, L. T. Duy, B. Y. Kim, B. U. Hwang, M. Jang, K. S. Shin, S. W. Kim and N. E. Lee, *Nanoscale*, 2014, **6**, 15144–15150.
30 A. Gao, N. Lu, P. Dai, C. Fan, Y. Wang and T. Li, *Nanoscale*, 2014, **6**, 13036–13042.
31 O. S. Kwon, H. S. Song, S. J. Park, S. H. Lee, J. H. An, J. W. Park, H. Yang, H. Yoon, J. Bae, T. H. Park and J. Jang, *Nano Lett.*, 2015, **15**, 6559–6567.
32 T. Q. Trung, N. T. Tien, D. Kim, M. Jang, O. J. Yoon and N. E. Lee, *Adv. Funct. Mater.*, 2014, **24**, 117–124.

33 M. Iwamura, N. Akizuki, Y. Miyauchi, S. Mouri, J. Shaver, Z. H. Gao, L. Cognet, B. Lounis and K. Matsuda, *ACS Nano*, 2014, **8**, 11254–11260.
34 J. I. Lee, S. H. Cho, S. M. Park, J. K. Kim, J. K. Kim, J. W. Yu, Y. C. Kim and T. P. Russell, *Nano Lett.*, 2008, **8**, 2315–2320.
35 S. Park, S. An, H. Ko, C. Jin and C. Lee, *ACS Appl. Mater. Interfaces*, 2012, **4**, 3650–3656.
36 Y. K. Park, W. Y. Rho, T. Mahmoudi and Y. B. Hahn, *Chem. Commun.*, 2014, **50**, 10502–10505.
37 L. L. Wang, J. N. Deng, Z. Lou and T. Zhang, *J. Mater. Chem. A*, 2014, **2**, 10022–10028.
38 H. Yoon, S. H. Lee, O. S. Kwon, H. S. Song, E. H. Oh, T. H. Park and J. Jang, *Angew. Chem., Int. Ed.*, 2009, **48**, 2755–2758.
39 J. A. Goding, A. D. Gilmour, P. J. Martens, L. A. Poole-Warren and R. A. Green, *J. Mater. Chem. B*, 2015, **3**, 5058–5069.
40 J. S. Lee, S. G. Kim, J. Jun, D. H. Shin and J. Jang, *Adv. Funct. Mater.*, 2014, **24**, 6145–6153.
41 Y. S. Hsiao, B. C. Ho, H. X. Yan, C. W. Kuo, D. Y. Chueh, H. H. Yu and P. Chen, *J. Mater. Chem. B*, 2015, **3**, 5103–5110.
42 J. W. Park, S. J. Park, O. S. Kwon, C. Lee and J. Jang, *Analyst*, 2014, **139**, 3852–3855.
43 Y. Wu, Y. X. Chen, J. Yan, S. Yang, P. Dong and P. Soman, *J. Mater. Chem. B*, 2015, **3**, 5352–5360.
44 S. Kumar, M. Willander, J. G. Sharma and B. D. Malhotra, *J. Mater. Chem. B*, 2015, **3**, 9305–9314.
45 X. Strakosas, M. Sessolo, A. Hama, J. Rivnay, E. Stavrinidou, G. G. Malliaras and R. M. Owens, *J. Mater. Chem. B*, 2014, **2**, 2537–2545.
46 O. S. Kwon, S. J. Park, H. Yoon and J. Jang, *Chem. Commun.*, 2012, **48**, 10526–10528.
47 W. K. Oh, S. Kim, H. Yoon and J. Jang, *Small*, 2010, **6**, 872–879.
48 J. W. Park, C. Lee and J. Jang, *Sens. Actuators, B*, 2015, **208**, 532–537.
49 X. M. Yang, Z. X. Zhu, T. Y. Dai and Y. Lu, *Macromol. Rapid Commun.*, 2005, **26**, 1736–1740.
50 L. Fan, G. Zhao, H. Shi and M. Liu, *Biosens. Bioelectron.*, 2015, **68**, 303–309.
51 R. Ansari, *E-J. Chem.*, 2006, **3**, 186–201.
52 M. Joulazadeh and A. H. Navarchian, *Synth. Met.*, 2015, **199**, 37–44.
53 J. Upadhyay, A. Kumar, B. Gogoi and A. K. Buragohain, *Synth. Met.*, 2014, **189**, 119–125.
54 J. Upadhyay and A. Kumar, *Mater. Sci. Eng., B*, 2013, **178**, 982–989.
55 Z. Lin, Y. Liu, Y. Yao, O. J. Hildreth, Z. Li, K. Moon and C. P. Wong, *J. Phys. Chem. C*, 2011, **115**, 7120–7125.
56 M. A. Pope, C. Punckt and I. A. Aksay, *J. Phys. Chem. C*, 2011, **115**, 20326–20334.
57 Y. Fang, B. Luo, Y. Jia, X. Li, B. Wang, Q. Song, F. Kang and L. Zhi, *Adv. Mater.*, 2012, **24**, 6348–6355.
58 S. W. Lee, N. Yabuuchi, B. M. Gallant, S. Chen, B. S. Kim, P. T. Hammond and Y. Shao-Horn, *Nat. Nanotechnol.*, 2010, **5**, 531–537.
59 Z. Zha, L. Xu, Z. Wang, X. Li, Q. Pan, P. Hu and S. Le, *ACS Appl. Mater. Interfaces*, 2015, **7**, 17837–17843.
60 S. Pei and H. M. Cheng, *Carbon*, 2012, **50**, 3210–3228.
61 J. Jun, J. S. Lee, D. H. Shin and J. Jang, *ACS Appl. Mater. Interfaces*, 2014, **6**, 13859–13865.
62 Y. S. Lee and B. K. Lee, *Carbon*, 2002, **40**, 2461–2468.
63 A. J. Plomp, D. S. Su, K. P. de Jong and J. H. Bitter, *J. Phys. Chem. C*, 2009, **113**, 9865–9869.
64 Y. C. Chiang, W. H. Lin and Y. C. Chang, *Appl. Surf. Sci.*, 2011, **257**, 2401–2410.
65 O. S. Kwon, S. H. Lee, S. J. Park, J. H. An, H. S. Song, T. Kim, J. H. Oh, J. Bae, H. Yoon, T. H. Park and J. Jang, *Adv. Mater.*, 2013, **25**, 4177–4185.
66 Q. Zhang, Y. Wang, A. Mateescu, K. Sergelen, A. Kibrom, U. Jonas, T. Wei and J. Dostalek, *Talanta*, 2013, **104**, 149–154.
67 O. A. Alsager, S. Kumar, B. Zhu, J. Travas-Sejdic, K. P. McNatty and J. M. Hodgkiss, *Anal. Chem.*, 2015, **87**, 4201–4209.

